Lymphatic abnormalities are associated with *RASA1* gene mutations in mouse and man

Patricia E. Burrows[a,1,2], Manuel L. Gonzalez-Garay[b,c,1], John C. Rasmussen[c,1], Melissa B. Aldrich[c], Renie Guilliod[d], Erik A. Maus[d], Caroline E. Fife[d,3], Sunkuk Kwon[c], Philip E. Lapinski[e], Philip D. King[e], and Eva M. Sevick-Muraca[c,4]

[a]Department of Diagnostic and Interventional Imaging, University of Texas Health Science Center at Houston, Houston, TX 77030; [b]Division of Genomics and Bioinformatics, University of Texas Health Science Center at Houston, Houston, TX 77030; [c]Center for Molecular Imaging, The Brown Foundation Institute of Molecular Medicine, University of Texas Health Science Center at Houston, Houston, TX 77030; [d]Center for Lymphedema Management, Memorial Hermann Hospital, Houston, TX 77030; and [e]Department of Microbiology and Immunology, University of Michigan Medical School, Ann Arbor, MI 48109

Edited by Rakesh K. Jain, Harvard Medical School and Massachusetts General Hospital, Boston, MA, and approved April 8, 2013 (received for review December 28, 2012)

Mutations in gene *RASA1* have been historically associated with capillary malformation–arteriovenous malformation, but sporadic reports of lymphatic involvement have yet to be investigated in detail. To investigate the impact of *RASA1* mutations in the lymphatic system, we performed investigational near-infrared fluorescence lymphatic imaging and confirmatory radiographic lymphangiography in a Parkes–Weber syndrome (PKWS) patient with suspected *RASA1* mutations and correlated the lymphatic abnormalities against that imaged in an inducible Rasa1 knockout mouse. Whole-exome sequencing (WES) analysis and validation by Sanger sequencing of DNA from the patient and unaffected biological parents enabled us to identify an early-frameshift deletion in *RASA1* that was shared with the father, who possessed a capillary stain but otherwise no overt disease phenotype. Abnormal lymphatic vasculature was imaged in both affected and unaffected legs of the PKWS subject that transported injected indocyanine green dye to the inguinal lymph node and drained atypically into the abdomen and into dermal lymphocele-like vesicles on the groin. Dermal lymphatic hyperplasia and dilated vessels were observed in Rasa1-deficient mice, with subsequent development of chylous ascites. WES analyses did not identify potential gene modifiers that could explain the variability of penetrance between father and son. Nonetheless, we conclude that the *RASA1* mutation is responsible for the aberrant lymphatic architecture and functional abnormalities, as visualized in the PKWS subject and in the animal model. Our unique method to combine investigatory near-infrared fluorescence lymphatic imaging and WES for accurate phenoptyping and unbiased genotyping allows the study of molecular mechanisms of lymphatic involvement of hemovascular disorders.

CM-AVM | lymphatics | near-infrared fluorescence imaging | indocyanine green imaging

The gene *RASA1* encodes for protein p120 Ras GTPase-activating protein (p120 RasGAP or RASA1) that regulates Ras activation and blood vessel growth in humans. Germ-line mutations in *RASA1* cause the autosomal dominant vascular disorder capillary malformation–arteriovenous malformation (CM-AVM), with high penetrance and variable expressivity [Online Mendelian Inheritance in Man (OMIM) no. 608354] (1–5). CMs are observed in all patients with *RASA1* mutations and present as single or multiple small pink cutaneous lesions. Fast-flow lesions that include AVMs, arteriovenous fistulas, and Parkes–Weber syndrome (PKWS) (OMIM no. 608355) are observed in one-third of cases. PKWS caused by *RASA1* mutation typically presents with symmetrical overgrowth of the involved extremity with large cutaneous CM and diffuse microshunting causing cardiac volume overload. Recent reports of upper- and lower-extremity lymphedema (6, 7), together with the finding that a small number of CM-AVM patients develop chylothorax and chylous ascites (5), indicate that lymphatic malformation may be an additional phenotype associated with mutations in *RASA1*. In mice, deletion of *Rasa1* causes embryonic lethality, as a result of abnormal blood vessel development. However, Lapinski et al. (8, 9) recently generated conditional *Rasa1* knockout mice in which loss of gene expression could be induced in adult animals either in all tissues or specifically within lymphatic endothelial cells (LECs). In both models, extensive overgrowth of the lymphatic vasculature was observed (8).

Techniques for imaging the lymphatic vasculature are not as developed or clinically implemented as they are for the blood vasculature using magnetic resonance (MR) and computed tomography (CT) angiography, and, as a result, the role of the lymphatics in vascular disorders is not well recognized. As part of a larger clinical study, we sought to use the investigational technique of near-infrared fluorescence lymphatic imaging (NIRFLI) to assess lymphatic architecture and dynamic function in normal control subjects and in subjects diagnosed with diseases in which lymphatic insufficiency may play a role. Herein, we present the rare case of a PKWS subject who we found possessed (*i*) an inactivating mutation in *RASA1*, (*ii*) abnormal lymphatics architecture and function compared with those imaged in normal healthy subjects, and, most striking, (*iii*) similar lymphatic characteristics as imaged in mice after induced deletion of *Rasa1*.

Results

NIRFLI and Radiographic Lymphangiography of a PKWS Subject. As part of a larger ongoing study in which we imaged 46 healthy control subjects and 96 subjects with suspected lymphatic disorders, we developed and used NIRFLI to assess the lymphatics of a 20-y-old male PKWS subject with an unknown genotype. At birth, the subject possessed a capillary stain on the back and left lower extremity with tissue and bony overgrowth, and at prepuberty, he developed lymphedema of the penis and left lower extremity, with lymphatic vesicles on his left foot, penis, and lower abdomen; the latter leaked whitish fluid (presumably chyle) (Fig. 1 *A–C*). No other family members had AVM or PKWS, but the father presented with a port wine stain on the left thigh (Fig. 1*D*).

Fig. 2 *A–C* shows the lower extremities of the PKWS subject and the circles denote the associated fields of view imaged by NIRFLI (depicted in Fig. 2 *D–F*) following intradermal administration of indocyanine green (ICG), a fluorescent dye which is immediately taken up by the initial lymphatics and is transported within the lymphatic vessels, enabling one to use fluorescent

Author contributions: P.E.B., M.L.G.-G., J.C.R., and E.M.S.-M. designed research; P.E.B., M.L.G.-G., J.C.R., M.B.A., R.G., E.A.M., C.E.F., S.K., and P.E.L. performed research; P.E.L. and P.D.K. contributed new reagents/analytic tools; M.L.G.-G., J.C.R., M.B.A., and S.K. analyzed data; and P.E.B., M.L.G.-G., J.C.R., P.D.K., and E.M.S.-M. wrote the paper.

The authors declare no conflict of interest.

This article is a PNAS Direct Submission.

[1]P.E.B., M.L.G.-G., and J.C.R. contributed equally to this work.

[2]Present address: Division of Vascular Interventional Radiology, Medical College of Wisconsin, Children's Hospital of Wisconsin, Milwaukee, WI 53226.

[3]Present address: St. Luke's Wound Clinic, The Woodlands, Texas, 77381.

[4]To whom correspondence should be addressed. E-mail: Eva.Sevick@uth.tmc.edu.

This article contains supporting information online at www.pnas.org/lookup/suppl/doi:10.1073/pnas.1222722110/-/DCSupplemental.

Fig. 1. Clinical photographs of the patient and his father. (*A*) Symmetrical overgrowth of left lower extremity with pale red cutaneous capillary stain. (*B*) Patient's left foot demonstrates swelling with lymphatic vesicles on digits (arrows). (*C*) Patient's right hand demonstrates capillary stain typical of CM-AVM (*RASA1* mutation). (*D*) Father's left lower extremity shows typical CM. Note pale margin.

imaging to noninvasively visualize lymph structures and dynamic lymph trafficking (10–13). In contrast to the typical collecting lymphatics of healthy control subjects that are straight, well-defined, and actively propel lymph through coordinated lymph vessel contraction and opening and closing of lymphatic valves (Fig. 3 *A–C* and Movies S1, S2, and S3), the lymphatics of the subject's unaffected right limb show abnormally dilated collecting lymphatics with sluggish lymph flow (Fig. 3 *D–F* and Movies S4, S5, and S6) while the initial lymphatics of the left affected limb of the PKWS subject are tortuous, appear ill-defined, and fail to efficiently transit ICG to collecting vessels with apparent extravascular drainage (Figs. 2 *D–F* and 4). Comparison of the left and right extremities, shown in a single whole field-of-view image depicted in Fig. 5*A*, demonstrates the lack of defined collecting lymphatics immediately associated with the capillary stain and CM-AVM lesion from the ventral view. The montage of images from the unaffected right limb shows abnormalities of lymphatic pooling in Fig. 5*B* demarked by arrows (see also Movie S5) that have not been seen in our studies of normal subjects. However, the montage of NIRFLI of the lateral left leg (affected, away from the capillary stain) shows dense networks of dilated, initial lymphatics on the foot, lower shin, and in the lateral knee (Fig. 5*C* and Movie S7). ICG-laden lymph drained into the genital and lower abdominal areas without clearly defined collecting lymphatics in the upper thigh and into subcutaneous lymphoceles that displayed intense fluorescence in the groin (Fig. 5*D* and Movie S8). The result suggests that peripheral lymph from both legs presumably mixes with the mesenteric lymph. Conducted a day later and under anesthesia before sclerotherapy, radiographic lymphangiography using water-based contrast indicated dilated collecting lymphatic vessels in the left lateral extremity (Fig. 6 *A* and *B*), and oily contrast confirmed NIRFLI results, demonstrating markedly dilated lymphatic channels in the left pelvis with reflux into the internal iliac lymphatics (Fig. 6 *C* and *D*). The cisterna chyli was visualized and appeared normal (Fig. 6*E*). The thoracic duct was not visualized. Lymphangiography was not performed on the unaffected right limb, and, thus, no confirmation of the abnormally dilated lymphatics observed from NIRFLI could be obtained in the unaffected limb.

Whole-Exome Sequencing and Sanger Sequencing of PKWS Subject and Parents. Although *RASA1* mutations are associated with PKWS, not all diagnosed PKWS subjects possess *RASA1* mutations. As a result, we conducted whole-exome sequencing on parents and probate to uncover other potential germ line-causative mutations and gene modifiers that may be responsible for the disease. Results from exome sequencing and bioinformatics analysis revealed that each of the members of the trio shared a similar number of variations (187,254 ± 3,121). We found 145 rare, nonsynonymous coding variants (NSCVs) in 132 genes, likely to be deleterious, shared only between father and son (Fig. S1 and Table S1). Of these variants, we found only one gene that belonged to the classic MAPK signaling pathway implicated in blood vascular disorders, *RASA1*. The *RASA1* mutation in both father and son is a 5-bp deletion that results in an early frameshift starting at codon 206 pI206fs (RASA1 is 1,047 aa in length). This mutation, validated with Sanger sequencing (Fig. S2), disrupts one copy of the gene leaving only one active copy of *RASA1*. Because the father also possessed a small capillary stain but no overt lymphatic phenotype, we searched for potential modifier genes passed from the mother that could explain the higher penetrance of the phenotype in the son. We found 138 NSCVs, in 122 genes, shared only between mother and son (Table S2); however, none of these 122 genes are currently known to interact with *RASA1* or participate in the MAPK signaling pathway.

NIRFLI Imaging of Inducible Rasa1 Knockout Mice. To further confirm the association between *RASA1* and lymphatic abnormalities, we conducted NIRFLI imaging of an adult induced Rasa1 knockout mouse (8, 9, 14). Fig. 7*A* shows the typical normal lymphatic structure of a $Rasa1^{fl/fl}$ [wild-type (WT)] mouse (injected with tamoxifen 8 wk previously) that drains from the base of the tail to the inguinal lymph node and through the conducting lymphatic vessel to the axillary lymph node. By contrast, in $Rasa1^{fl/fl}$ $Ub^{ert2cre}$ mice that carry the conditional floxed *Rasa1* allele ($Rasa1^{fl/fl}$) and a ubiquitin-driven ert2cre transgene ($Ub^{ert2cre}$), at 8 wks after tamoxifen administration and before any overt phenotype has been observed, the lymphatic architecture dramatically changes with the appearance of "budding" initial lymphatic capillaries (Fig. 7*B*). In addition, Fig. 7*C* shows that 8 wk after induced *Rasa1* deletion but before the onset of chylothorax, which occurs in all animals, ICG-laden lymph is "leaked" into the peritoneal cavity and fluoresces in ill-defined vessels in the genital and lower abdominal areas, similar to the phenotype observed in the PKWS subject with an inactivating *RASA1* mutation. Histology shows that after Rasa1 loss, initial and collecting lymphatic vessels are significantly dilated (8). Movies S9, S10, and S11 demonstrate the lymphatic drainage as a function of time after intradermal ICG administration and show that contractile motion of the collecting and conducting lymphatics remains intact, consistent with our past studies (8).

Discussion

The unidirectional lymphatic vasculature is an integral part of the circulatory system. Besides its critical role for immune

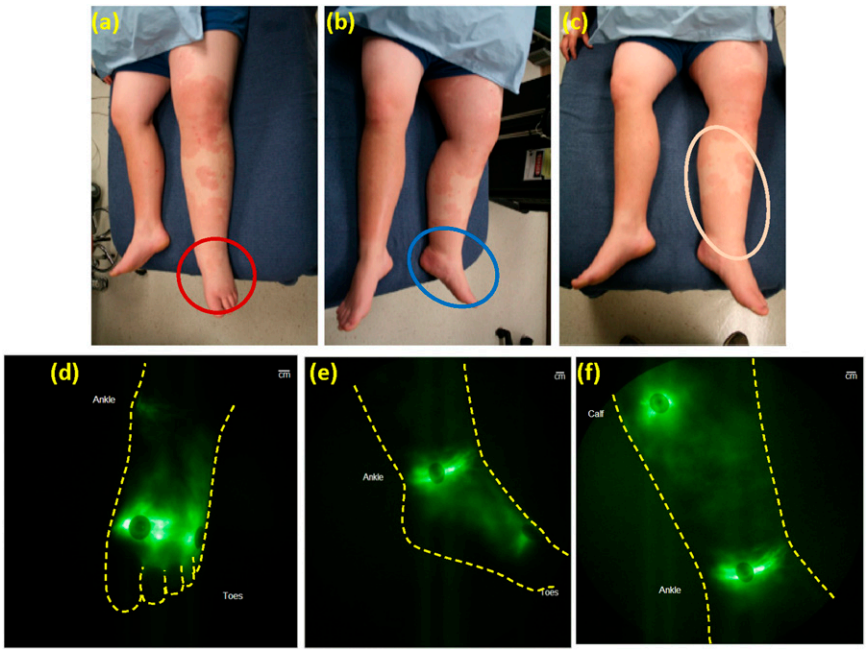

Fig. 2. Dorsal (*A*) and medial (*B* and *C*) views of stain on left leg with circles indicating fields of view for corresponding dorsal (*D*) and medial (*E* and *F*) views from NIRFLI.

surveillance and fat absorption in the gut, the lymphatic circulation is critical to the normal functioning of the blood vasculature. Excess fluid and macromolecules that permeate from blood capillaries into the interstitial space are taken up by the initial lymphatics and transited by collecting or conducting lymphatic vessels for return to the blood vasculature thereby maintaining fluid and oncotic homeostasis. When the lymphatics are compromised or overwhelmed by enhanced rates of blood capillary filtration, increased interstitial fluid accumulation and pressure results, which, in turn, produces tissue edema and elevated blood pressure. In addition, the developing lymphatic vasculature arises from the cardinal vein and the collecting lymphatic vessels and, like blood vessels, are comprised of a single layer of LECs surrounded by vascular smooth muscle cells. Initial lymphatics are characterized by a lack of smooth muscle cells [for review, see Alitalo (15)]. Given the function and developmental relationship between the lymphatic and blood vasculatures, it may not be surprising that aberrant lymphatic structure and function accompany vascular malformations.

***RASA1* Is Associated with Lymphatic Abnormalities in Mouse and in Man.** The heterozygous *RASA1* mutation found in the PKWS subject and his father is expected to result in a loss of RASA1 function and unregulated Ras activation (16). The mutation is significant because it allows direct comparison with phenotypes of animal models in which Rasa1 is deficient or Ras is overexpressed. First, overexpression of Ras in LECs within mice has been shown to cause edema and chylothorax (17), suggesting the loss of Ras regulation arising from Rasa1 deficiency could result in aberrant lymphatics. Using NIRFLI, we showed hyperplasia of the initial lymphatics, dilation of initial and collecting lymphatics, contractility of conducting or collecting lymphatics, chylothorax, and, in some cases, chylous ascites after inducing Rasa1 loss in adult mice. Using both NIRFLI and radiographic lymphangiography in the PKWS subject with an inactivating *RASA1* mutation. Although no blood vasculature phenotype is observed upon loss of Rasa1 in adult mice, it is observed in Rasa1-deficient embryos, suggesting that early gene loss may be required for blood vascular defects and that a Rasa1 deficiency imposed later in life may be more impactful to the lymphatic vasculature as opposed to the hemovasculature. Because the animal models show that lymphatic malformation results from loss of Rasa1 in LECs themselves (8), Rasa1-mediated lymphatic abnormalities may also occur independently of blood vascular malformation. In the PKWS subject studied, radiographic lymphangiography showed no evidence of lymphatic obstruction but did show retrograde flow in dilated pedal and internal iliac lymphatics. The vesicles, or cutaneous lymphatics, in the groin contained chyle (intestinal lymphatic fluid) but filled with fluorescent contrast that had been injected in the lower extremity. These results suggest a mispatterning of peripheral and mesenteric lymphatics, mixing of peripheral lymph and chyle because of insufficiency of hypertropic lymphatic channels or perhaps a combination thereof.

Given the lack of a single case of homozygous *RASA1* mutations in subjects reported in the literature, a strong negative selection exists for homozygous mutations in man, consistent with the embryonic lethality of homozygous *Rasa1* deletion in mice. In the conditional knockout mouse used, deletion of the exon that encodes the part of the RasGAP protein essential for catalytic activity results in the loss of expression of catalytically active RasGAP. In fact, we have shown previously that the cre-mediated recombination of the floxed allele results in complete loss of mRNA and protein expression as a consequence of nonsense-mediated RNA decay (14). The frameshift mutation found in our two subjects starts at codon 206 (p.206fs), which is in the first Src Homology 2 (SH2) domain of the protein. Therefore, at most, a severely truncated protein would result. More likely, however, the mutation would result in a complete null allele because an in-frame stop codon close to the mutation would predictably also result in nonsense-mediated RNA decay of transcripts.

Variable Expressivity of *RASA1* Mutation Remains to Be Explained. Because the father of the proband also possessed a small capillary stain but no overt lymphatic phenotype, potential modifier genes passed from the mother were sought, but none was found. Because the father did not agree to lymphatic phenotyping with NIRFLI, we were unable to determine whether he harbored a subtle, abnormal lymphatic contribution of the disease that could be directly related to the *RASA1* mutation in this instance. Hence, there remains no direct evidence for the variable penetrance of phenotype in this family. The answer to why the heterozygous loss of *RASA1* function in humans gives a lymphatic phenotype, whereas homozygous postdevelopmental loss of RASA1 in mice is necessary for the lymphatic phenotype remains a subject for investigation. In humans, Vikkula and coworkers (5) have suggested that a somatic second hit in the unaffected *RASA1* allele

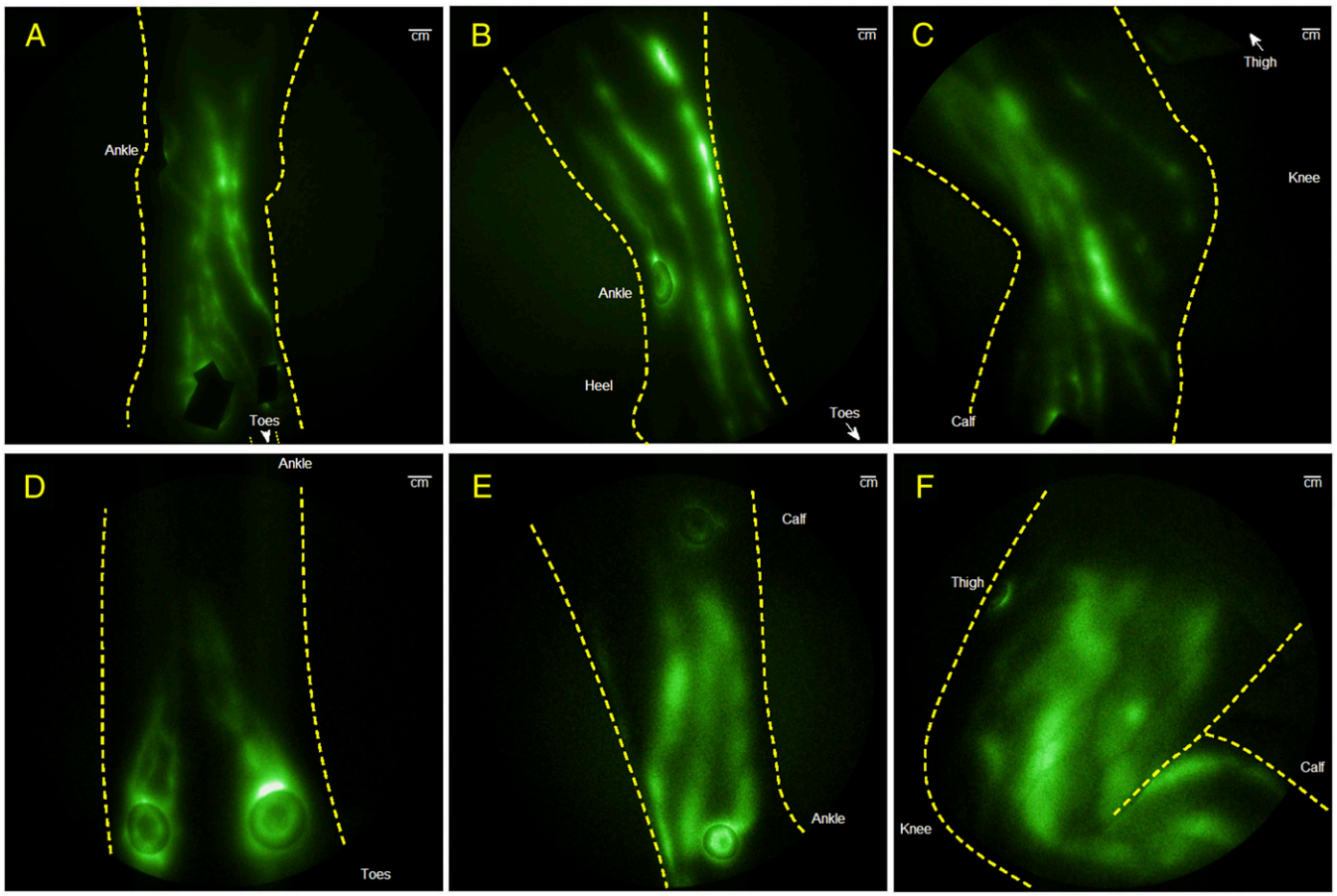

Fig. 3. (*A–C*) Typical NIRFLI depicting the normal collecting lymphatics on the dorsum of the foot of a 48-y-old female (Movie S1), medial views of ankle/calf of a 47-y-old male (Movie S2), and the knee of a 43-y-old male (Movie S3). (*D–F*) NIRFLI on the right, unaffected leg of the PKWS subject depicting lymphatics on the dorsum of the foot and medial views of dilated lymphatic vessels in the ankle/calf and knee. See Movies S4, S5, and S6 for sluggish propulsive flow.

could result in total loss of *RASA1* expression in development and that it is these cells that give rise to abnormal vessels for a paradominant inheritance pattern. If this hypothesis is correct, then the heterozygous mutations in humans may be considered comparable to the induced homozygous Rasa1-deficient mouse, except that fewer cells in the human are homozygous *RASA1*-null and the expressivity is variable in humans, whereas not in the homozygous mouse.

Nonetheless, assuming that the *RASA1* genotype–phenotype association is conserved across species, this individual case suggests that there is a lymphatic component to CM-AVM (5, 7) that may be evaluated from lymphangiography and investigational NIRFLI.

Investigational NIRFLI. NIRFLI is estimated to detect lymphatic vasculatures as deep as 3–4 cm from the tissue surface with trace intradermal doses of near-infrared fluorescent dye (18, 19) but is unable to visualize deeper lymphatic structures such as the cisterna chyli or thoracic duct in adults, as is possible with MR or CT lymphangiography. Nonetheless, NIRFLI enabled assessment of dilated collecting lymphatics of both affected and unaffected limb, of which the former results were confirmed through MR lymphography using water- and oil-based contrast administration. Unlike MR or CT lymphangiography, there is no need for lymphatic cannulation for trace near-infrared fluorophore administration that could potentially aggravate lymphatic disease. In addition, because of the high fluorescent photon-count rates, NIRFLI acquisition is rapid, enabling compilation of sequential images to form movies of propulsive lymph transport that result from contractility of lymphatic vessels.

Implications for Assessing Lymphatic Component to Hemovascular Disorders. The routine clinical use of NIRFLI for rapid assessment of lymphatic abnormalities could clarify the lymphatic component and enable identification and more accurate phenotyping of lymphovascular disorders. Although the genotype and phenotype associations between the single PKWS subject and animal model are striking, it is important to note that PKWS is a rare disorder and nonsynonymous variants in *RASA1* are extremely rare. To date, the largest exome sequencing project (ESP) of 6,500 DNA samples shows only 12 amino acid changes for a total of 20 mutated *RASA1* alleles, without a single mutation corresponding to the far more severe deletion reported herein and by Revencu et al. (5). As a consequence, this study was limited to one subject whose abnormal lymphatic phenotype was not followed during the course

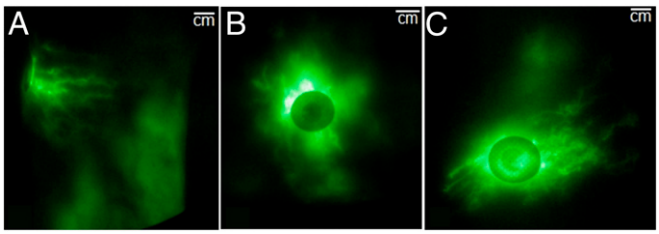

Fig. 4. ICG injection sites on the medial ankle (*A*), lateral calf (*B*), and thigh (*C*) on the left affected limb showing hyperplasia of presumed initial lymphatics. To prevent oversaturation of the camera system, the injection sites are covered with an adhesive bandage.

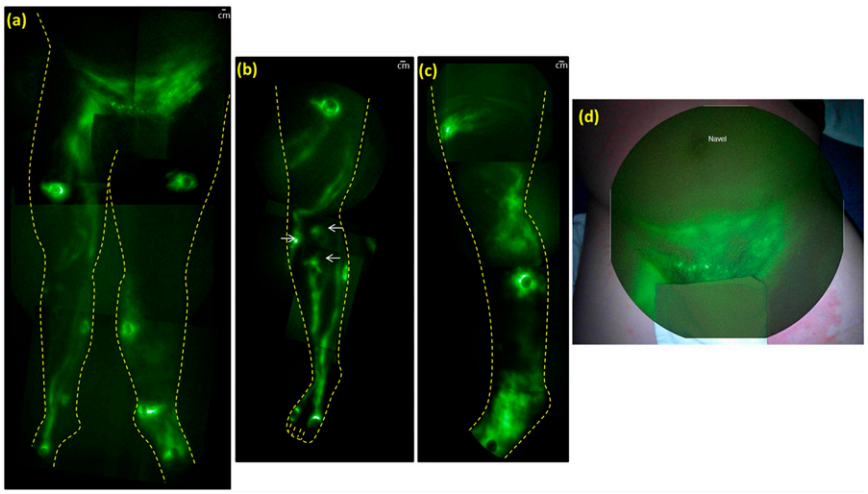

Fig. 5. (*A*) NIRFLI montage of right (unaffected) and left (affected) limbs. (*B*) NIRFLI montage showing abnormal lymph pooling (arrows) in right unaffected limb. (*C*) NIRFLI montage showing abnormal lymphatic on the lateral side of the affected limb (Movie S7). (*D*) NIRFLI overlaid on white light to show lymphatic drainage into groin and pelvic region with lymphoceles displaying bright fluorescence (Movie S8).

of disease progression. Nonetheless, given that the similar lymphatic vessel abnormalities are observed in ubiquitous and LEC-specific Rasa1-deficient mice, the imaging results presented herein suggest that *RASA1* mutation may be directly responsible for an aberrant lymphatic component to the blood vascular disorder of CM-AVM. Because there is a paucity of safe and routine clinical diagnostics of the lymphatics, the extent of lymphatic involvement in hemovascular disorders is probably underestimated. By combining new imaging techniques for accurate clinical phenotyping of the lymphatics, next generation sequencing for unbiased variant discovery, and transgenic animal models, we are able to further study the molecular mechanisms of lympho- and hemovascular disease.

Materials and Methods

The NIRFLI protocol used for this human imaging study was conducted under Investigational New Drug Application 102,827 for off-label use of ICG and was funded by the National Heart, Lung, and Blood Institute (NHLBI) of the National Institutes of Health (Clinical Trials no. NCT00833599: "Imaging Lymphatic Function in Normal Subjects and in Persons with Lymphatic Disorders"; www.clinicaltrials.gov). The Health Insurance Portability and Accountability Act-compliant study was approved by the Institutional Review Board at the University of Texas Health Science Center at Houston and its affiliated clinical site (Memorial Hermann Hospital). Informed consent was obtained. The animal studies were conducted under the University of Michigan and the University of Texas Health Science Center at Houston Animal Welfare Committees. All other procedures were conducted as standard of care.

DNA Collection and Analysis. DNA was extracted from blood using Paxgene Blood DNA Kit (PreAnalytix) according to the vendor's instructions. Two micrograms of genomic DNA were submitted to Axeq Technologies for human exome capture sequencing using TrueSeq 62-Mb target enrichment (Illumina) (20). Approximately 63,000,000 reads of an average size of 107 bp per sample was returned to us as two fastq files (one file per orientation).

Each pair of fastq files was aligned to human genome (hg19) using Novoalign (Novocraft Technologies; www.novocraft.com), keeping parameters at the default settings, as recommended by Novocraft Technologies. SAMtools (http://samtools.sourceforge.net) (21) was used to sort the SAM files, create BAM files, and generate their index files. Picard (SourceForge; http://picard.sourceforge.net) was used to remove all of the PCR duplicates from the BAM files. The Genome Analysis Toolkit (GATK) Version 2.2 (22) was used for local realignments, base quality recalibration, and variant calling. Parameters were set as described in GATK's Best Practices. GATK generated standard variant call format (VCF) files [1000 Genomes Project VCF Version 4; www.1000genomes.org/wiki/Analysis/Variant%20Call%20Format/vcf-variant-call-format-version-41]. The VCF files were annotated using SnpEff (23) and ANNOVAR (24). From this point onward, we focused only on the putative coding nonsynonymous variants. To filter out common variants and sequencing errors, all of the low-quality variants were first removed using the following heuristic: (*i*) variants without a minimum coverage of 10×; (*ii*) variants without a minimum average Phred quality score of 30; (*iii*) variants located at the beginning or at the end of all of the reads; (*iv*) variants without a minimum average mapping quality of 60; and (*v*) variants with coverage of more than 300× and triallelic.

All of the information necessary to remove the variants was extracted from the corresponding BAM file using the python wrapper for SAMtools, pysam (Python interface for the SAM/BAM sequence alignment and mapping format; http://code.google.com/p/pysam). Common variants were removed using allele frequency information from the NHLBI ESP (http://evs.gs.washington.edu/EVS). A common variant was defined as a variant present in the ESP with a minor allele frequency of more than 1%. Every variant was annotated for potential functional effects in the protein using three variant effect predictors: SIFT (25), PolyPhen-2 (Prediction of functional effects of human nsSNPs; http://genetics.bwh.harvard.edu/pph2) (26), and MutationTaster (www.mutationtaster.org) (27). After a list of low-frequency nonsynonymous coding variants was generated for each sample, a segregation analysis was performed to determine which variants were present only in the father and son. Identified variants were then confirmed through Sanger sequencing. For Sanger sequencing, two pairs of primers were designed using Oligo 7 and synthesized by Integrated DNA Technologies to validate the *RASA1* mutation [set 1: TCCCCTAGGTGGTATCACGG (forward) and AAATGGTTGACAACATTCATCTGG (reverse); and set 2: CAAGTGTCCATAGAAATTCTGCAC (forward) and AACAAGCTTCCTTCTCTATTATTTGTTACT (reverse)]. Polymerase chain reactions (PCRs) were performed using the Kapa HiFi HotStart ReadyMix DNA Polymerase (no. KK2602; KapaBiosystems) according to the manufacturer's instruction. To visualize DNA fragments, 5 μL of the PCR product was loaded on a 1% agarose gel (or Lonza 1.2% by weight agarose Flash Gel); ethidium bromide was used for the staining. Purification of the

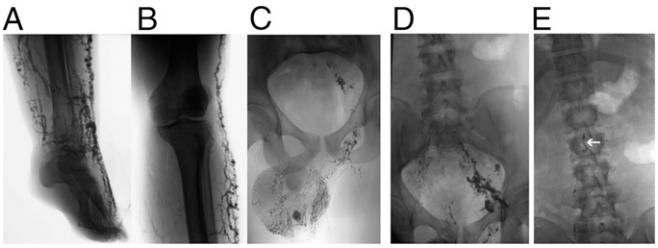

Fig. 6. Radiographic imaging of collecting lymphatic channels of left extremity. Injection of water-soluble contrast medium after ultrasound guided cannulation of dilated lymphatic channel in the left foot demonstrates marked dilation of lymphatic channels in the foot (*A*) and in the left lateral calf (*B*). (*C*) Injection of oily contrast medium (Lipiodol) after cannulation of scrotal lymphatic channel with sonographic guidance is shown (note dilated lymphatic channels and retrograde filling of lymphatic cyst). (*D*) Pelvis after injection of additional Lipiodol through more proximal lymphatic channel; left pelvic lymphatics are dilated with reflux (contrast filled syringe is visible). (*E*) image of abdomen after opacification of cisterna chyli (arrow), which is normal in size. Thoracic duct was not well visualized.

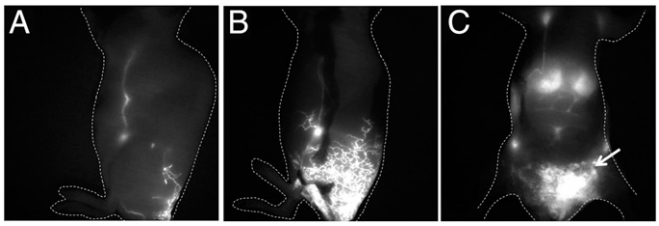

Fig. 7. (*A*) Normal lymphatic vasculature of a *Rasa1*$^{fl/fl}$ mouse 26 s after ICG administration at the base of the tail (Movie S9). (*B*) Abnormal lymphatic architecture of inducible *Rasa1* knockout 117 s after ICG administration at the base of the tail (Movie S10). The phenotype occurs months before onset of chylous ascites and chylothorax (8). Results shown are typical of n= 10 *Rasa1*$^{fl/fl}$ and n = 10 *Rasa1*$^{fl/fl}$*Ub*^{ert2cre} mice. (*C*) Ventral view showing hyperplasia in lower abdominal region and leaked ICG in the gut (arrow), indicating chylous ascites (Movie S11).

DNA was done using Qiagen Gel Extraction Kit (no. 28706) following the manufacturer's instruction. Purified PCR products were sequenced at the MD Anderson Cancer Center sequencing facility using a 3730XL DNAnalyzer (Applied Biosystems).

ICG Administration and NIRFLI. ICG (Pulsion Medical Systems) was diluted in saline to achieve a concentration of 250 μg/mL, and six intradermal injections of 0.1 mL were administered using 31-gauge needles on the feet, medial ankle, medial and lateral shins, and dorsal thigh at roughly the same locations on each leg of the conscious PKWS and normal control subjects. Immediately after administration, investigational NIRFLI commenced. Vital signs were monitored at 15–30 min intervals for 2 h (the duration of the imaging session), and follow-up monitoring at 24 h after administration indicated there was no indication of allergic response. NIRFLI was conducted as reported previously (11, 13, 19, 28) using a military-grade, night vision goggle-intensified CCD and laser diode system. Tissue surfaces were illuminated with less than 1.9 mW/cm^2 of 785-nm excitation light, and 512 × 512 resolution images were collected with 200-ms exposure times to visualize dynamic lymphatic pumping action.

Radiographic Lymphoscintigraphy. Radiographic lymphangiography was carried out on the day following NIRFLI, under general anesthesia, and at the time of sclerotherapy of the leaking lymphatic vesicles. A large lymphatic channel in the left foot was cannulated with sonographic guidance using a 21-gauge needle. Water-soluble contrast medium was injected, and images were recorded from the left foot to thigh. They demonstrated dilated but otherwise normal morphology of the superficial lymphatics. To better determine the etiology of the chylous reflux, lymphangiography using oily contrast medium (Lipiodol, Guerbet) was injected into the dilated lymphatic channels in the left scrotum and perineum, with radiographic imaging of the pelvis, abdomen, and thorax.

NIRFLI of *Rasa1* Mice. *Rasa1*$^{fl/fl}$*Ub*^{ert2cre} and control *Rasa1*$^{fl/fl}$ mouse strains have been described previously (8). Briefly, in the former but not latter strain, *Rasa1* expression is extinguished in all tissues following administration of tamoxifen to adult mice on 2 consecutive days (10 μL/g; 0.2 mg/g; i.p.). Anesthetized animals (n = 10, *Rasa1*$^{fl/fl}$; n = 10, *Rasa1*$^{fl/fl}$*Ub*^{ert2cre}) underwent NIRFLI before and for up to 20 wk after tamoxifen injection to monitor changes in lymphatic phenotype as a result of RASA1 loss. Although the imaging procedures are described in detail elsewhere (29), imaging consisted of intradermal administration of ICG to the base of the tail and collection of NIRFLI images with exposure times of 200–800 ms. There were no overt abnormal phenotypes observed other than the lymphatic abnormalities detected through NIRFLI before the animal succumbed to chylothorax.

ACKNOWLEDGMENTS. We acknowledge the assistance of Otis Hall, Holly Robinson, Karen Gore, I-Chih Tan, and Banghe Zhu in the collection of the animal and subject imaging. This work was supported, in part, by National Institutes of Health Grants R01 HL092923 (to E.M.S.-M.), R01 CA128919 (to E.M.S.-M.), and R01 HL096498 (to P.D.K.) and American Heart Association Grant 11POST7580023 (to P.E.L.).

1. Boon LM, Mulliken JB, Vikkula M (2005) RASA1: Variable phenotype with capillary and arteriovenous malformations. *Curr Opin Genet Dev* 15(3):265–269.
2. Eerola I, et al. (2003) Capillary malformation-arteriovenous malformation, a new clinical and genetic disorder caused by RASA1 mutations. *Am J Hum Genet* 73(6): 1240–1249.
3. Hershkovitz D, Bercovich D, Sprecher E, Lapidot M (2008) RASA1 mutations may cause hereditary capillary malformations without arteriovenous malformations. *Br J Dermatol* 158(5):1035–1040.
4. Hershkovitz D, Bergman R, Sprecher E (2008) A novel mutation in RASA1 causes capillary malformation and limb enlargement. *Arch Dermatol Res* 300(7):385–388.
5. Revencu N, et al. (2008) Parkes Weber syndrome, vein of Galen aneurysmal malformation, and other fast-flow vascular anomalies are caused by RASA1 mutations. *Hum Mutat* 29(7):959–965.
6. Behr GG, et al. (2012) CM-AVM syndrome in a neonate: Case report and treatment with a novel flow reduction strategy. *Vasc Cell* 4(1):19.
7. de Wijn RS, et al. (2012) Phenotypic variability in a family with capillary malformations caused by a mutation in the RASA1 gene. *Eur J Med Genet* 55(3):191–195.
8. Lapinski PE, et al. (2012) RASA1 maintains the lymphatic vasculature in a quiescent functional state in mice. *J Clin Invest* 122(2):733–747.
9. Lapinski PE, Qiao Y, Chang CH, King PD (2011) A role for p120 RasGAP in thymocyte positive selection and survival of naive T cells. *J Immunol* 187(1):151–163.
10. Kwon S, Sevick-Muraca EM (2007) Noninvasive quantitative imaging of lymph function in mice. *Lymphat Res Biol* 5(4):219–231.
11. Rasmussen JC, Tan IC, Marshall MV, Fife CE, Sevick-Muraca EM (2009) Lymphatic imaging in humans with near-infrared fluorescence. *Curr Opin Biotechnol* 20(1):74–82.
12. Sharma R, et al. (2007) Quantitative imaging of lymph function. *Am J Physiol Heart Circ Physiol* 292(6):H3109–H3118.
13. Tan IC, et al. (2011) Assessment of lymphatic contractile function after manual lymphatic drainage using near-infrared fluorescence imaging. *Arch Phys Med Rehabil* 92(5):756.e1–764.e1.
14. Lapinski PE, et al. (2007) Generation of mice with a conditional allele of the p120 Ras GTPase-activating protein. *Genesis* 45(12):762–767.
15. Alitalo K (2011) The lymphatic vasculature in disease. *Nat Med* 17(11):1371–1380.
16. King PD, Lubeck BA, Lapinski PE (2013) Nonredundant functions for Ras GTPase-activating proteins in tissue homeostasis. *Sci Signal* 6(264):re1.
17. Ichise T, Yoshida N, Ichise H (2010) H-, N- and Kras cooperatively regulate lymphatic vessel growth by modulating VEGFR3 expression in lymphatic endothelial cells in mice. *Development* 137(6):1003–1013.
18. Sevick-Muraca EM (2012) Translation of near-infrared fluorescence imaging technologies: Emerging clinical applications. *Annu Rev Med* 63:217–231.
19. Sevick-Muraca EM, et al. (2008) Imaging of lymph flow in breast cancer patients after microdose administration of a near-infrared fluorophore: Feasibility study. *Radiology* 246(3):734–741.
20. Illumina (2011) TruSeq Exome Enrichment Kit. Datasheet: Sequencing (Illumina, San Diego). Available at www.illumina.com/documents/products/datasheets/datasheet_truseq_exome_enrichment_kit.pdf.
21. Li H, et al.; 1000 Genome Project Data Processing Subgroup (2009) The Sequence Alignment/Map format and SAMtools. *Bioinformatics* 25(16):2078–2079.
22. McKenna A, et al. (2010) The Genome Analysis Toolkit: A MapReduce framework for analyzing next-generation DNA sequencing data. *Genome Res* 20(9):1297–1303.
23. Cingolani P, et al. (2012) A program for annotating and predicting the effects of single nucleotide polymorphisms, SnpEff: SNPs in the genome of Drosophila melanogaster strain w1118; iso-2; iso-3. *Fly (Austin)* 6(2):80–92.
24. Wang K, Li M, Hakonarson H (2010) ANNOVAR: Functional annotation of genetic variants from high-throughput sequencing data. *Nucleic Acids Res* 38(16):e164.
25. Kumar P, Henikoff S, Ng PC (2009) Predicting the effects of coding non-synonymous variants on protein function using the SIFT algorithm. *Nat Protoc* 4(7):1073–1081.
26. Adzhubei IA, et al. (2010) A method and server for predicting damaging missense mutations. *Nat Methods* 7(4):248–249.
27. Schwarz JM, Rödelsperger C, Schuelke M, Seelow D (2010) MutationTaster evaluates disease-causing potential of sequence alterations. *Nat Methods* 7(8):575–576.
28. Rasmussen JC, et al. (2010) Human lymphatic architecture and dynamic transport imaged using near-infrared fluorescence. *Transl Oncol* 3(6):362–372.
29. Kwon S, Sevick-Muraca EM (2011) Non-invasive, dynamic imaging of murine intestinal motility. *Neurogastroenterol Motil* 23(9):881–e344.